MDPI

Article

Impact of Design Parameters on the Dynamic Response and Fatigue of Offshore Jacket Foundations

Ali Marjan [1,*] **and Phil Hart** [2]

1   Renewable Energy Marine Structures, School of Water, Energy, and Environment, Cranfield University, Cranfield, Bedford MK43 0AL, UK
2   Energy and Sustainability, School of Water, Energy, and Environment, Cranfield University, Cranfield, Bedford MK43 0AL, UK
*   Correspondence: ali.marjan@cranfield.ac.uk; Tel.: +44-1234-758249

Abstract: The lifetime of offshore foundations is governed by a combination of harsh environmental conditions and complex service loads. The fatigue limit state (FLS) analysis needs to be performed in the time domain to capture the complex phenomenon. This study aims to investigate different parameters and design modifications that can impact the design life of an offshore jacket foundation. An OC4 jacket foundation is designed in industrial software from DNV and reduced to a super-element model. The super-element model is connected to an NREL 5-MW wind turbine designed in Bladed. The time-series loads are used to compute the fatigue damages faced by the foundation during the service life. The impact of soil non-linearity, marine growth, scour size, the mass of the transition piece, and the grouted connection's design on the dynamic response and fatigue damages are compared. A 30% increase in life was observed by replacing the concrete transition piece with a lightweight steel configuration. The fatigue damages were considerably greater for the inclined pile in the leg grouted connection than for the leg in the pile concept. The study provides a different perspective by analysing the effect of design parameters and design changes in the complex and computationally expensive time-series domain.

Keywords: wind turbine; jacket; offshore; fatigue; Bladed; FLS; transition piece; grouted connection; OC4

1. Introduction

The International Renewable Energy Agency (IRENA) claims that wind power will provide more than 33% of global electricity demand by 2050 [1]. Many countries are establishing very large offshore wind farms in a quest to meet their clean energy targets. The total installed wind energy capacity in Europe from Offshore Wind Turbines (OWT) has increased from 84 GW in 2010 to 189 GW in 2018 [2]. In order to speed up the adoption and reduce the cost, there is a need to constantly improve the design of OWT foundations.

An OWT faces a combination of complex loads throughout life, and fatigue life is the main performance criterion of OWT foundations [3]. The complexity and computationally expensive nature of time-series fatigue analysis force the researchers to make simplified assumptions, which impacts the accuracy of modern-day research. A complete wind resource analysis was done in [4] to describe the method of reference site selection. The study also highlighted the method of correlating short-term data with multi-year historical data to extract the environmental data for any research. The environmental data, including the wind and wave resource information, is needed to perform any time-series fatigue simulation. The author discusses the preliminary design of monopile foundations to support larger wind turbines and deeper water in [5]. A time-series wind field was generated in the TurbSim, but the study only focused on DLC (Design Load Case) 1.2 and ignored conditions above cut-off wind speed and wave currents.

The soil-structure interaction is a key player in offshore foundation modelling and is discussed in [6]. The industry standard definition of pile-soil interaction is inaccurate

for offshore foundations with a large diameter (monopile). The effect on the fatigue life of monopile foundations was studied using four soil foundation models in [7], which resulted in the variation of fatigue damage up to 22% based on different soil models. The PISA project proposed a different soil-pile definition method based on field testing and numerical results [8]. However, the method only shows good accuracy at the testing site and can not be used on other or multi-layered soils. A detailed FEA analysis was performed in [9] based on five constraints (fatigue, stress, vibration, buckling, and deformation). It was observed that fatigue performance is the primary design driver of the jacket foundations. Abdulhakim et al. studied the structural reliability of the jacket subjected to corrosion fatigue [10]. The spectral fatigue analysis method was used on an eight-legged oil and gas jacket foundation and showed that 73 joints had a service life of fewer than 20 years [11]. The research was performed to study the effect of design parameters and foundation types (fixed base, monopile, and caisson) on the dynamic response and fatigue in [12]. However, the fatigue analysis was performed in a MATLAB-based tool (MLife) and did not include the time series aspect. A study was performed to analyse modelling parameters' effect on the jacket foundation's dynamic response [13], but the effect on fatigue life was not considered. The author also compared the dynamic response of monopile, jacket, and tripod foundation in [14] without including the complex time-series fatigue phenomenon. The structural redundancy's effect on fatigue life and life extension was studied in [15]. The author proposes using the fracture mechanics approach along with the fatigue analysis in the future. Thanh-Tuan et al. presented a cost-effective three-legged jacket by studying various bracing patterns. The dynamic response was significantly changed with the change in the bracing pattern [16]. The dynamic responses of monopile and jacket foundations were compared in [17]. It was observed that the jacket foundation had a better dynamic response, and the monopile foundation was not suitable for the Korean offshore wind farm.

An integrated or super-element design approach can be used for time-series fatigue analysis. A previous study compared integrated and super-element approaches in [18] and found similar fatigue damages. The same set of software was used to perform fatigue analysis of a 10-MW wind turbine using an integrated design approach in [19]. It was observed that integrated or super-element approaches could be used alternatively. When combined with hydro-servo-elastic software (e.g., Bladed), the computational time can be significantly reduced, resulting in improved fatigue analysis accuracy due to the interaction of the whole model. The most used OWT foundations are monopile and jacket foundations. Monopiles are primarily used for shallow water with depths up to 30 m. The jacket foundations, on the other hand, can be successfully used for water depths above 40 m. Moreover, jacket foundations can be used in multi-layered soil, but monopiles are mostly used in sand and gravel soils. The primary objective of this research is to establish the effect of various parameters on the jacket foundation's dynamic response and fatigue life. This study focuses on a super-element method, where an OC4 jacket foundation in a 50 m water depth, modelled in Sesam, is reduced to the super-element file. The super-element model provides information on the model's mass matrix, gravity vector, and stiffness matrix. The super-element model includes the values of these parameters at the interface point (intersection of tower and TP). The interface point is then shared with the Bladed software to compute the time series of forces and moments in three axes. The time-series of loads are imported in the Sesam Wind Manager (SWM) to generate a time-series of stress range, eventually used to determine fatigue damages. The process is repeated on similar environmental conditions for a set of parameters and design modifications to obtain their effect on the dynamic response and fatigue damages. This paper contributes to knowledge with a unique set of changes in the design, material of transition piece, and grouted connection, and observes their effect on the dynamic response and fatigue life. The study also includes comprehensive details of the complex design of FLS analysis using the super-element method.

The paper is organised as follows. Section 2 describes the reference model. Section 3 explains the model validation methodology. Section 4 explains the methodology used for FLS analysis. Section 5 discusses the results, and Section 6 concludes the study.

1.1. Sources of Loads

An offshore wind turbine faces a series of complex loads during its service life. The design standards DNV-OS-J101 [20] and IEC 61400-3 [21] suggest the list of loads to consider while performing analysis. The DNV-RP-C205 [22] standard was used to calculate each environmental load. The loads faced by an offshore wind turbine are usually classified into the following groups.

1.1.1. Inertia Loads

The loads are encountered due to the mass of Rotor Nacelle Assembly (RNA), Transition Piece (TP), tower, and foundation. These loads contribute most to the buckling and significantly affect the modal analysis. The structure can fail if an OWT encounters resonance due to the poor design, emphasising the need to consider these loads during the design process.

1.1.2. Wind Loads

The wind loads caused by the drag change with the height and the mean wind speed. The power-law profile is used to examine wind speed variation with height using Equation (1).

$$\overline{V}(z) = \overline{V}_r \left(\frac{z}{z_r} \right)^\alpha \tag{1}$$

where, $\overline{V}_r$ shows the wind speed at the hub height and α shows the roughness coefficient, usually 0.115 for offshore conditions. The wind loads as a function of height can be calculated by using Equation (2). Where $D(z)$ represents the tapered diameter of the tower and $C_{D,T}$ shows the drag coefficient of the tower at any height z.

$$F_{twr}(z) = \frac{1}{2} \rho_a C_{D,T} D(z) \, \overline{V}_r^2(z) \tag{2}$$

1.1.3. Rotor's Aerodynamic Loads

Due to airflow interaction, the combination of static and dynamic loads acting on the wind turbine rotor generates aerodynamic loads. The loads faced by the rotor are transferred to the top of the tower. The values of these loads for this study were obtained from [23] to perform the modal analysis.

1.1.4. Current Loads

Like the wind loads, the current loads are height and drag-dependent. Morison's equation describes the sub-surface current velocity by an exponential profile from MSL to the seabed. Where d is the water depth from MSL to the seabed and $V_{c,MSL}$ is the current velocity at MSL [24].

$$V_c(z) = V_{c,MSL} \left(\frac{d+z}{d} \right)^{1/7} \tag{3}$$

1.1.5. Hydrostatic Load

The offshore foundation is immersed in seawater, which results in hydrostatic pressure. The hydrostatic load (F_h) is a permanent normal load that increases with depth (h) and can be calculated by Equation (4), where g is the gravitational constant.

$$F_h = \rho_w g h \tag{4}$$

1.1.6. Wave Loads

Morison's equation is used because the wavelength, sea depth, shape, and size of an offshore jacket foundation are all governed by drag. The diameter D of the jacket's member must be smaller than one-fifth of the wavelength for Morison's equation to be employed. The current and wave loads can be computed for the structure submerged in the water by using Morison's equation [25]. Where C_m and C_d are inertia and drag coefficients, D is the member's diameter, U_x and a_x are velocity and acceleration induced by the current and wave.

$$F = F_d + F_m = \frac{1}{2}\rho_w C_d D|U_x|U_x + \rho_w C_m \frac{\pi D^2}{4}a_x \tag{5}$$

2. Reference Model

2.1. Site Specifications

The site-specific data used in this study is from the K-13 deep water site. The site is located in the North Sea and has a water depth of 50 m. The wind and wave climate definition is discussed in detail in Upwind Design Basis [26] and has been used by many studies due to the availability of data and validation purposes. According to the Pierson-Moskowitz wave spectrum, the wave conditions are characterised by the peak spectral period and significant wave height. Important site-specific data are summarised in Table 1. A peakedness factor of 1.0 was used for fatigue load cases, and a factor of 3.3 was used for all other cases, as advised in [26]. For simplicity, the effect of wind-wave directionality and turbulence intensity has not been considered.

Table 1. Site-specific data.

Parameter	Value
50-year significant wave height	9.4 m
50-year max wave height	17.48 m
50-year max wave period	10.87 s
Reference wind speed	42.73 m/s
Marine growth (-2 to -40 m)	100 mm
Marine growth density	1100 kg/m^3
Normal current at MSL	0.6 m/s
Extreme current at MSL	1.2 m/s

2.2. Wind Turbine Model

The study focuses on the NREL 5-MW baseline offshore wind turbine, described by Jonkman et al. in [27]. The wind turbine was developed for research and conceptual studies to assess the effect of offshore wind energy in deep and shallow water. The model was developed by combining publicly available data from the Repower 5M prototype, the Multibird M5000, and the projects like WindPACT, RECOFF, and DOWEC. The model has widely been used by many projects (Upwind Design Basis [26], IEA Wind Annex OC3 [28], and OC4 projects [29]) for code comparison and to standardise baseline offshore wind turbines.

The NREL 5-MW wind turbine is an upwind, three-bladed horizontal axis wind turbine. The hub height is 87.5 m. Moreover, the tower mass is centred along the tower centerline. The main dimensions and characteristics of the turbine are given in Table 2.

2.3. FEA Model

The FEA model of the jacket and soil was developed in the Genie (version 8.0-11) module of Sesam software, which has widely been used in the industry for research and development purposes. The analysis is performed on the developed model based on the site-specific conditions, such as wind, wave, and current loads. The steps involved in developing the model and the definition of the foundation model are discussed in the following sections.

Table 2. NREL 5-MW specifications [27].

Rotor		Tower	
Diameter	126 m	Height	87.6 m
Rotor orientation	Upwind	CM location	38.234 m
Hub height (OC4)	90.55 m	Diameter top	3.87 m
Rated rotor speed	12.1	Diameter bottom	6 m
Number of blades	3	Thickness top	0.019 m
Drivetrain		Thickness bottom	0.027 m
Generator rotational speed	1173.7 RPM	**Masses**	
Rated rotor speed	12.1	Tower	347,460 kg
Gearbox ratio	97:1	RNA	350,000 Kg
Operational data		Hub mass	56,780 kg
Cut-in speed	3 m/s	Blade mass	17,740 kg
Rated wind speed	11.4 m/s		
Cut-out wind speed	25 m/s		
Rated power	5 MW		

2.3.1. Jacket Support Structure Model

This study focuses on the jacket-type foundation, usually four-legged and connected with braces through welded joints. The wind turbine is attached to the jacket support structure used in phase 1 of the OC4 project. The material properties, node coordinates, and member properties are the same as in the study [4]. The four levels of X-braces are connected with the four-legged jacket, and piles have a penetration depth of 45 m. The jacket has a total height of 70.15 m, including the TP (transition piece), which is 4 m high. The main properties of the OC4 jacket support structure are given in Table 3. The model was developed in Genie based on the provided information. The colour-coded Jacket support structure showing different cross-sections is given in Figure 1.

Table 3. OC4 jacket support structure parameters.

Component	Value
Steel density	7850 kg/m^3
Young's modulus	2.1×10^{11} N/m^2
Poisson's ratio	0.3
Number of legs	4
Water depth	50 m
X and mud braces OD, thickness	0.8 m, 20 mm
Lowest level leg OD, thickness	1.2 m, 50 mm
2nd to 4th level legs OD, thickness	1.2 m, 35 mm
Leg connecting TP OD, thickness	1.2 m, 40 mm
Pile OD, thickness	2.082 m, 60 mm
Jacket height above the mudline (including TP.)	70.15 m

2.3.2. Grouted Connection

The base model in the OC4 project only considers the jacket above the mudline, and only the section of piles above the mudline is considered. This implies that all six degrees of movement are considered zero. The pile has a bigger diameter and is connected with the leg by filling grout material between the surfaces. The grout materials density is 2000 kg/m^3. The grout connection volume from mean sea level –45 to –49.5 m is considered rigid in the model due to very high stiffness (Figure 2). The grouted connection is shown in black colour in Figure 1.
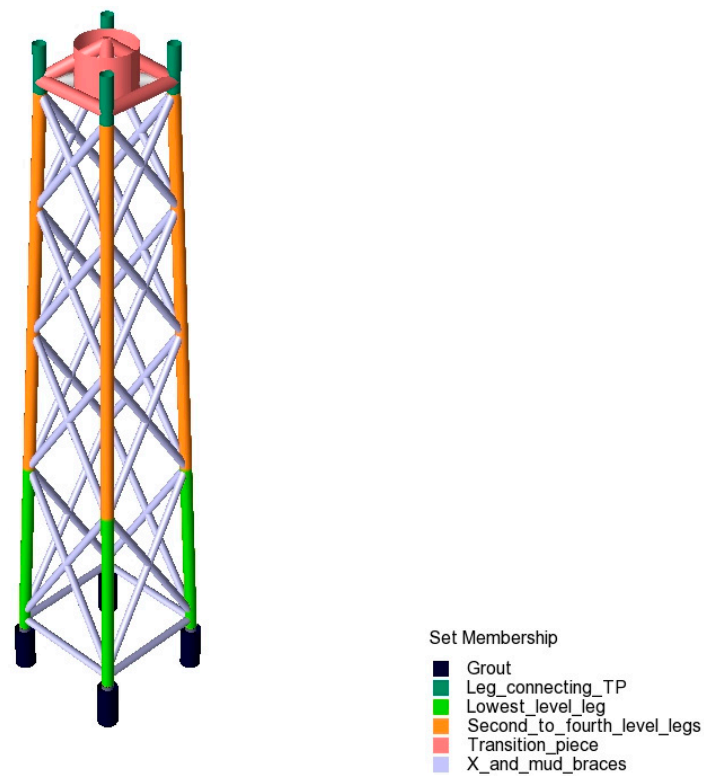
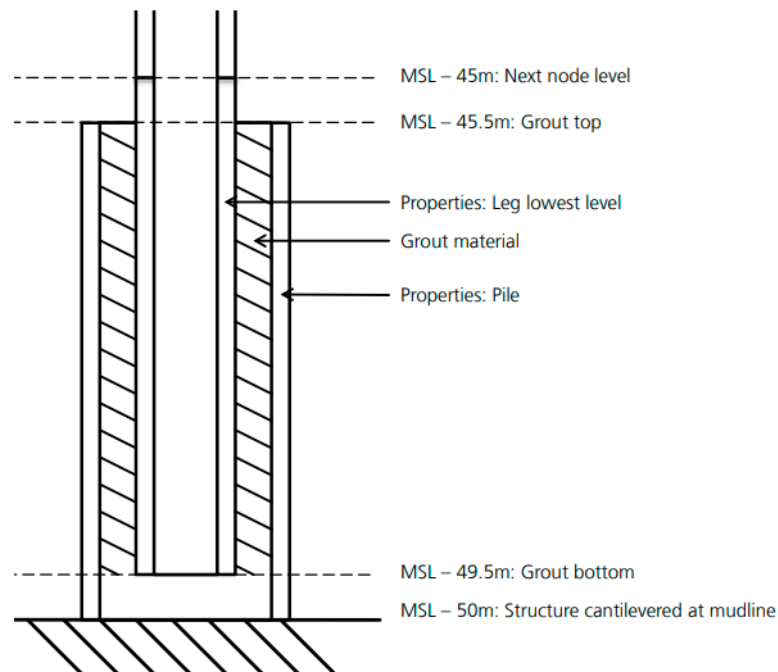**Figure 1.** Model of the jacket foundation.

Figure 2. A grouted connection between pile and leg [29].

This rigid model was used to perform the linear analysis, while the non-linear analysis was performed by including the soil and pile model. This is explained further in the following sections.

2.3.3. Transition Piece

The OC4 model considers the TP a rigid concrete block with a mass of 666 t. However, Genie lacks the ability to model a concrete block. The TP was, therefore, modelled as a

beam with increased stiffness to simulate a similar effect (see Figure 1). Moreover, point mass was included to obtain a total mass of 666 t.

2.3.4. Soil-Structure Interaction Modelling

The laterally loaded piles are mostly modelled with a simplified method called Beam on Nonlinear Winkler Foundation (BNWF) or a p-y method. The method provides simplicity and saves computational costs over the 3D FEA model. The hypothesis is that the soil reaction (p) exerted by the soil at the pile is proportional to the pile displacement (y). This method is widely used in the offshore oil & gas industry to find pile deformations and stiffness and is given in API and DNV industry standards. Although this approach has been widely used for the oil & gas industry design, its accuracy is questionable for offshore foundations having a large diameter (such as monopile). The study by [7] has determined that the p-y method overestimates the displacement, stiffness, and bending moment more than the FE methods for monopile. However, this study uses the p-y method to model the soil because it is reasonably accurate for slender bodies (such as jacket foundations) and provides good computational efficiency. The importance of proper soil-structure interaction for jacket foundations is discussed in [30]

The analysis is performed in the K-13 deep-water site. The six-layered soil profile of the site given in Table 4 was modelled in the Genie. The complete model showing the tower, jacket, piles, and six-layered soil is shown in Figure 3.

Table 4. The soil profile of k-13 deep-water site [26].

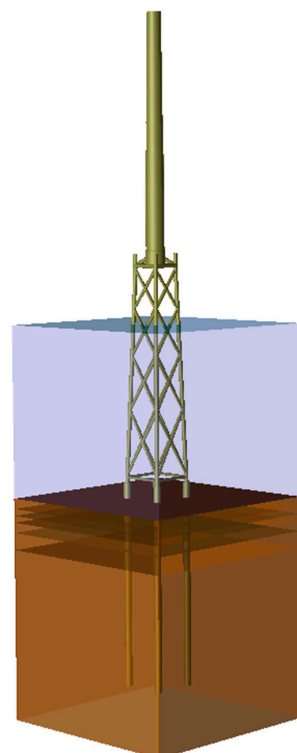|	Unit Weight (N/m^3)	Friction Angle (°)	Young's Modulus (Mpa)
0–3	10,000	36	30
3–5	10,000	33	30
5–7	10,000	26	50
7–10	10,000	37	50
10–15	10,000	35	50
15–50	10,000	37.5	80

Figure 3. Complete 3D model.

3. Model Validation

3.1. Modal Analysis

The modes of vibration were determined for a fixed foundation and non-linear pile-soil model. It is crucial to design semi-rigid (fixed at the base with some mobility like a jacket foundation in soil) so that the first natural frequency does not approach the 1P and 3P regions to avoid resonance. Figure 4 shows that the system's natural frequency with the NREL 5-MW wind turbine should be between 0.22 and 0.35 Hz [31]. The modal frequencies of the model with fixed base and non-linear model with soil were computed and compared with the existing literature. The first four frequencies of the fixed foundation were compared with [32], and the frequencies for both non-linear pile-soil models were compared with [33]. The results are compared in Table 5, where the second side-to-side bending (−9.1%) depicts the maximum deviation. This confirms the validity of the model.
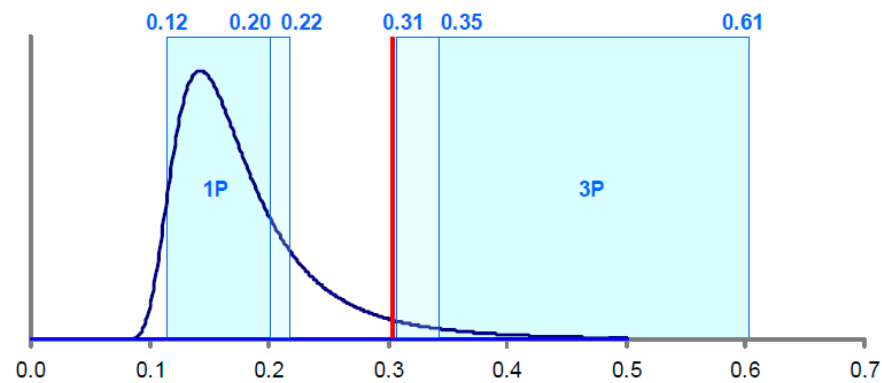

Figure 4. The power density of the NREL 5-MW wind turbine [26].

Table 5. Comparison of natural frequencies with the reference values.

Models	Natural Frequencies (Hz)			
	1st Fore-Aft	**1st Side-to-Side**	**2nd Fore-Aft**	**2nd Side-to-Side**
Fixed base [This study]	0.3169	0.3169	1.1799	1.1799
Fixed base [32]	0.3189	0.3189	1.1936	1.1936
Non-linear soil [This study]	0.2935	0.2935	0.935	0.937
Non-linear soil [33]	0.2772	0.2795	0.8931	1.023

3.2. Static Analysis

The deflection behaviour of the structure was assessed with static analysis and compared with the results given in [32]. The maximum displacement at the RNA was observed for comparison under the loaded conditions. Table 6 shows a good agreement with the literature, with a minor difference of −0.36%, further validating the model.

Table 6. Static deformation of the baseline wind turbine model.

Load Case RNA Mass/Thrust	Displacement at RNA		
	Present	**Ref. [32]**	**% Difference**
350 Tonne/2 MN	1.2045 m	1.2089	−0.36%

The contour plot of the deformation of the whole model and the graph of tower deflection along its length, with a fixed foundation, is shown in Figure 5.
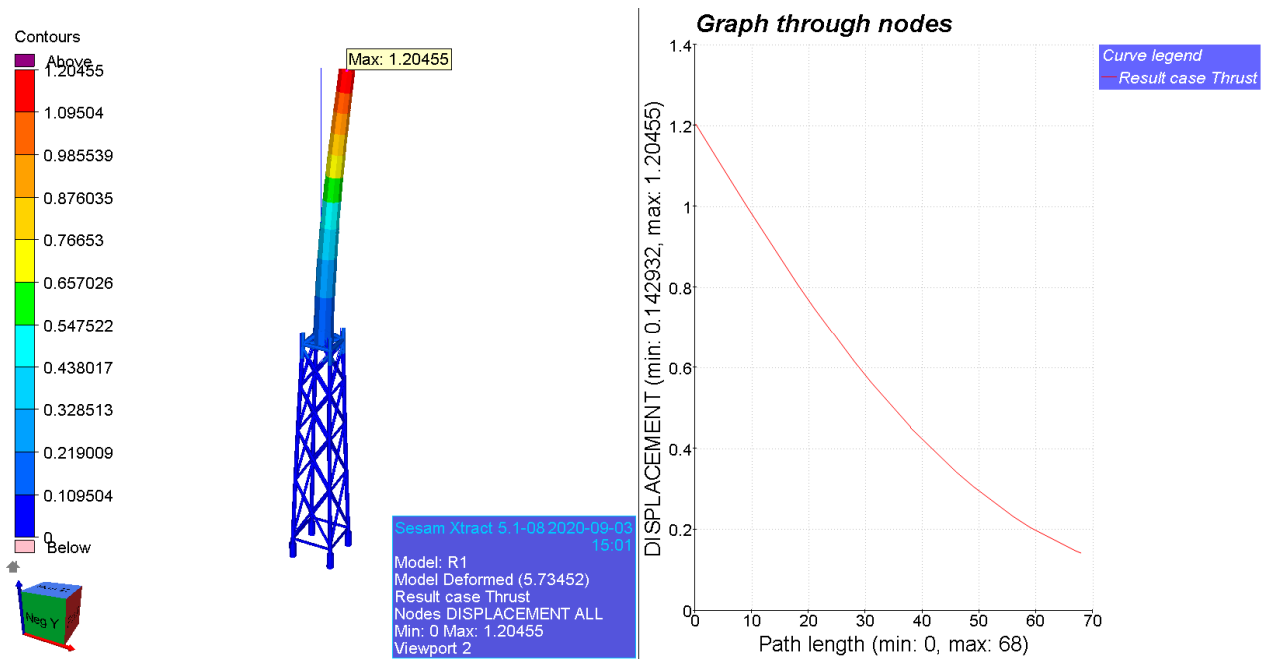
Figure 5. Deflection with a fixed base.

4. Fatigue Limit State (FLS) Analysis

The fatigue design of OWT support structures is controlled by the dynamic response to combined aerodynamic and hydrodynamic loads [34]. The S-N curve and fracture mechanics approaches are the two most often used fatigue assessment techniques. As advocated by the standards [35,36], the S-N curve method is the focus of this research. The S-N curve, which is based on experimental data and is a plot of Stress S against the number of cycles N, is used to calculate the fatigue failure of an object. The experiments are repeated for many similar specimens under stress to obtain the design S-N curve. The stress range at a point is related to the number of cycles to failures with the help of Equation (6). Where *N* is the number of cycles to failure, *m* is the negative inverse slope of the S-N curve, σ is the stress, and *C* is the intercept of the S-N curve with the log of the number of cycles *N*. This analysis involves estimating stress concentration factors (SCFs) for tubular joints based on geometry and butt welds. The fatigue life is based on the rainflow counting of stress time histories [37].

$$log_{10}(N) = C - m log_{10} \Delta\sigma \tag{6}$$

4.1. Methodological Approach for FLS

The FLS analysis is performed based on the super-element approach, which is discussed later. The FLS load calculation is based on the Design Load Cases (DLCs) recommended by [36]. FLS analyses are typically performed for DLC 1.2, DLC 6.4, and DLC 7.2. This study focuses on the DLCs given in Table 7, and DLC 7.2 (idling after fault) is omitted because most of the fatigue life is based on these DLCs only. Moreover, a reduced form of scatter diagram in the North-sea (in Table 8) is used to obtain the result due to the increased number of simulations to observe the effect of different parameters on the time-series fatigue life.

Table 7. Design load cases.

Design Load Case	Description	Type
DLC 1.2	Power production	FLS
DLC 6.4	Idling	FLS

Table 8. Scatter diagram.

Wind Speed (m/s)	Wave Height (m)	Period (s)	Occurrences/yr (h)	DLC
4	1.11	4.15	4365	DLC 1.2
14	1.90	4.30	2185	DLC 1.2
24	3.42	5.51	545	DLC 1.2
2	1.08	4.25	1260	DLC 6.4
30	4.46	6.25	410	DLC 6.4

The validated foundation model in Section 4.1 was exported to the SWM, where the Wajac input file defined the hydrodynamic properties, and Sestra defined the type of analysis. The super-element files were generated based on the input data.

4.1.1. Super-Element Design Method

Sesam offers time-series FLS analysis in integrated and super-element approaches. The entire structure (including the tower) is modelled in Genie and exported to Bladed (version 4.12) to generate time-series loads in an integrated design approach. The study [38] uses an integrated design approach on a 10-MW offshore wind turbine. However, in the super-element approach, only the jacket and the wave loads are exported to Bladed in the form of a super-element.

The super-element method is implemented in this research because it is extensively used in the industry due to the lack of a requirement to share the jacket design and the ability to export complex designs [39]. The super-element model should behave similarly to the integrated model. DNV has published verification studies showing the accuracy of the super-element method in [40]. Moreover, integrated and super-element approaches are compared in [18]. Figure 6 shows the schematic of the super-element method.
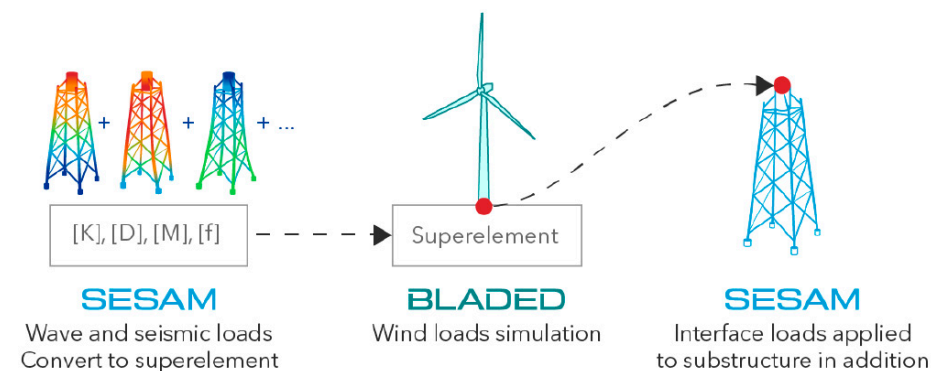

Figure 6. Super-element method [39].

The super-element files contain the model's mass matrix, gravity vector, and stiffness matrix information. The damping matrix was generated based on the Rayleigh coefficients, stiffness, and mass matrices. The original model was verified with the literature, as discussed in Section 3. However, the super-element data must also be converged (spectral and spatial) to replace the original model.

Spectral Convergence

The boundary node is at the interface point and contains only six degrees of freedom (DOFs) which is not enough. The number of DOFs is increased until there is an agreement between the dynamic response of the original model and the super-element model. The number of modes was selected after the dynamic response converged and was similar to the modal shapes based on the standalone jacket model in Genie. Hence, 40 additional DOFs were added to the super-element model to capture actual dynamic responses based on the original model. The verification report suggests that using 40 or more modes may reduce the difference between the two models to a maximum of 0.5%. Genie is used to obtain the eigenvalue frequencies of the jacket (excluding RNA and tower), and SWM obtains the

super-element model's frequencies. The model's modal frequencies are compared for the first 20 modes in Table 9 and show a maximum difference of only 0.16%. It shows that both models can be used interchangeably to produce similar responses.

Table 9. Comparison of modal frequencies of the original and super-element models.

Model Number	Original Model Freq. (Hz)	Super-Element Model Freq. (Hz)	Difference (%)
1	1.0885	1.0887	−0.01837
2	1.0885	1.0887	−0.01837
3	5.0687	5.07	−0.02565
4	6.1037	6.106	−0.03768
5	6.1038	6.106	−0.03604
6	6.7875	6.8139	−0.38895
7	7.4895	7.4896	−0.00134
8	9.0797	9.0791	0.006608
9	9.4819	9.4845	−0.02742
10	9.4821	9.4847	−0.02742
11	9.7622	9.7631	−0.00922
12	11.125	11.126	−0.00899
13	11.816	11.835	−0.1608
14	12.681	12.684	−0.02366
15	12.695	12.7	−0.03939
16	13.05	13.06	−0.07663
17	13.215	13.223	−0.06054
18	13.216	13.223	−0.05297
19	14.121	14.122	−0.00708
20	14.375	14.377	−0.01391

Spatial Convergence

In order to perform the super-element analysis, the super-element model should also show spatial convergence, i.e., show similar behaviour under the same loading condition. A simulation is performed in SWM on the original model under a specific load, and displacement at the interface point is noted. Moreover, another simulation is performed on a super-element model to observe the displacement at the interface node under the same loading conditions. The results are compared in the Xtract module at t = 25 s and show good accuracy, as shown in Figure 7.
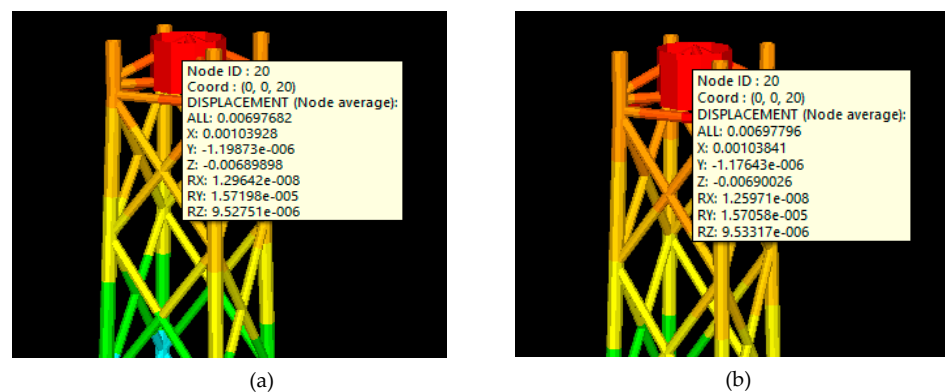

(a)

(b)

Figure 7. Comparison of nodal displacements for spatial convergence. (**a**) Displacements at the interface node of the original model. (**b**) Displacements at the interface node of the super-element model.

4.1.2. Bladed

An aero-hydroservo-elastic solver like Bladed is needed to simulate the coupled dynamic response of an offshore wind turbine. This complex simulation captures the interaction of a multi-physics system and simulates a holistic model in a coupled manner [41]. For defining the wind loads, each wind speed is simulated for a period of 200 s. The

turbulence can be modelled in the software to include temporal and spatial variations. The wind loads in this study are simulated by ignoring any variations in the wind because of the computational cost. Turbine wake is not modelled in such simulations because only one wind turbine is being simulated. Although the super-element approach excludes hydro-servo interaction, the verification report [40] shows similar results by integrated and super-element approaches [42]. This super-element model was exported, where it was attached at the interface point to the NREL 5-MW wind turbine. NREL 5-MW wind turbine was fully defined in Bladed, including blade geometry, airfoil sections, rotor, hub, nacelle, and tower.

The Bladed software can generate simple time-series loads with the built-in controller. However, the fatigue damages were relatively high because of the complex nature of FLS analysis. The light and dark blue lines (Figure 8) show demanded generator speed and torque and are constant initially. However, the measured generator speed (orange) fluctuated around the demanded generator speed later in the simulation. The controller tries to correct this by pitching the blades (the green line fluctuates between 0 and 20°), but it over-corrects and exacerbates the oscillation in generator speed. An external controller for the NREL 5-MW wind turbine was implemented to improve the accuracy of fatigue results. Figure 9 shows the stabilised blade pitch angle for a demanded generator torque. It shows the need to design and implement an external controller to improve the accuracy of complex FLS simulations. It was also observed that the blade pitch angle increases at higher wind speeds but remains constant at a given wind speed.
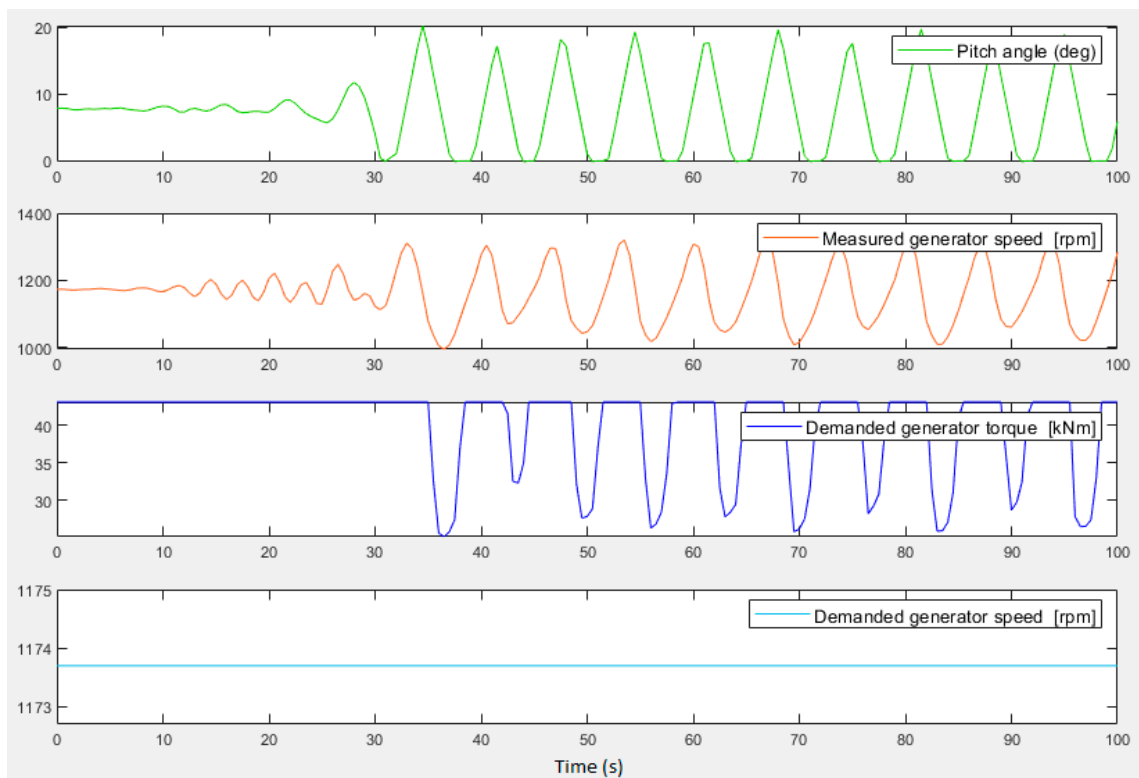

Figure 8. Error in blade's pitch angle with a built-in controller.

4.1.3. FLS Simulation

The time-series load data from Bladed was then exported to SWM again to generate time-series stress. There are several methods to model the wave loads, as described in [43,44]. However, the structures having strong dynamic responses, like OWTs, require stochastic modelling of the sea states and their kinematics [45]. The significant wave height and mean crossing period define the wave energy spectra characteristics for OWTs [19]. The wave energy spectra for this study are given in Table 8. The stress concentration

factors (SCF) were calculated based on the Efthymiou principle on each tubular joint. The calculation of SCFs considers the joint's geometry and the nature of applied loads. The software uses the method to calculate SCF as given in the standard DNVGL-RP-C203 [44]. Based on the SCFs and the time series of loads, stresses on the joints are calculated based on the hotspot stress approach. Figure 10 shows the location of hotspots on the brace. The highest value of the eight locations on the circumference for each simulation was selected for the calculations [38]. Miner's rule was used to calculate the total damage at each joint after obtaining the time series of stress ranges. The calculation of damages is based on a user-selected S-N curve. Figure 11 shows the flowchart of modules used to generate fatigue time-series results.
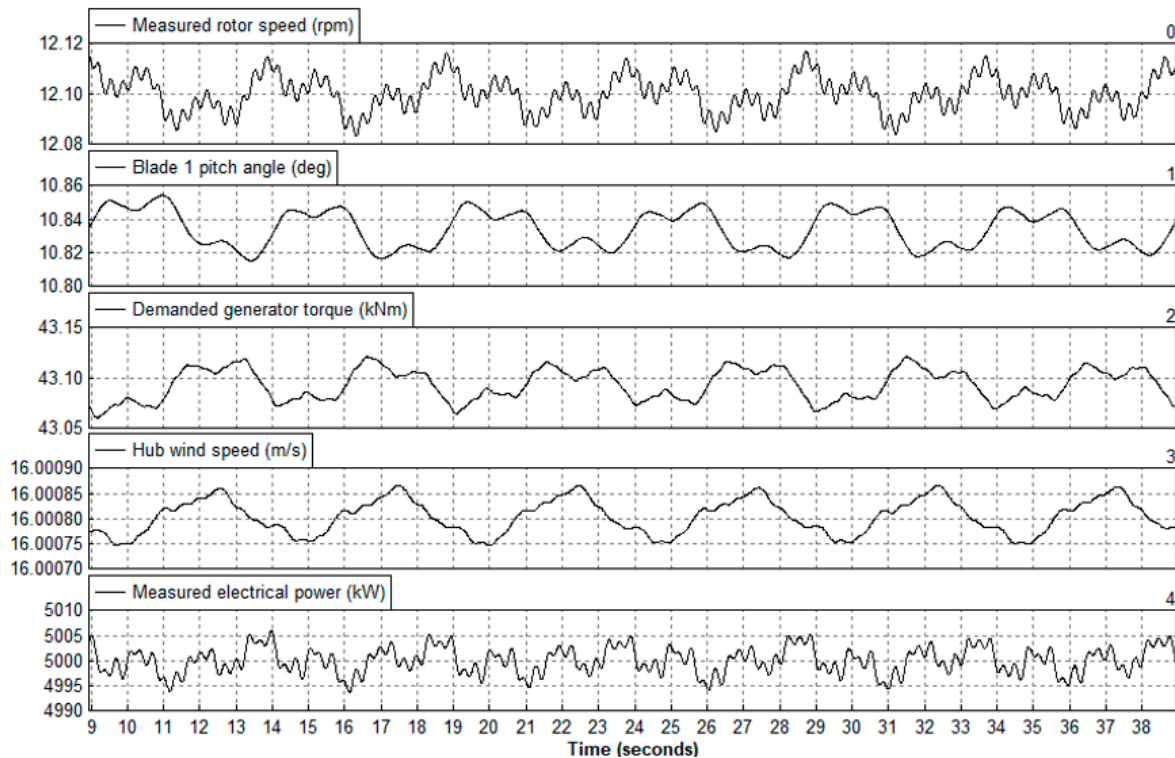

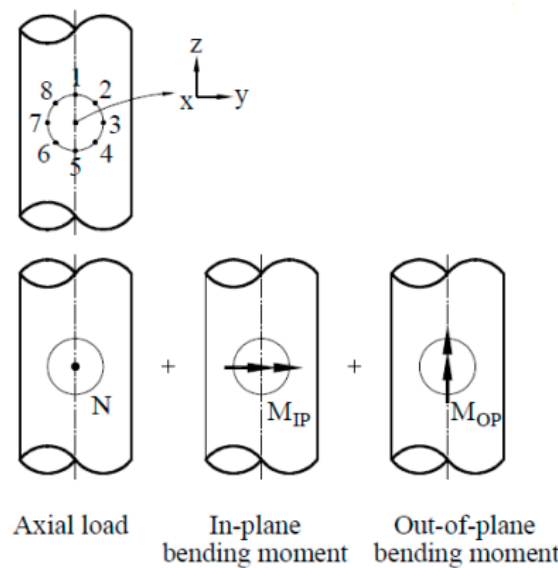**Figure 9.** Uniform blade pitch angle with the designed controller.

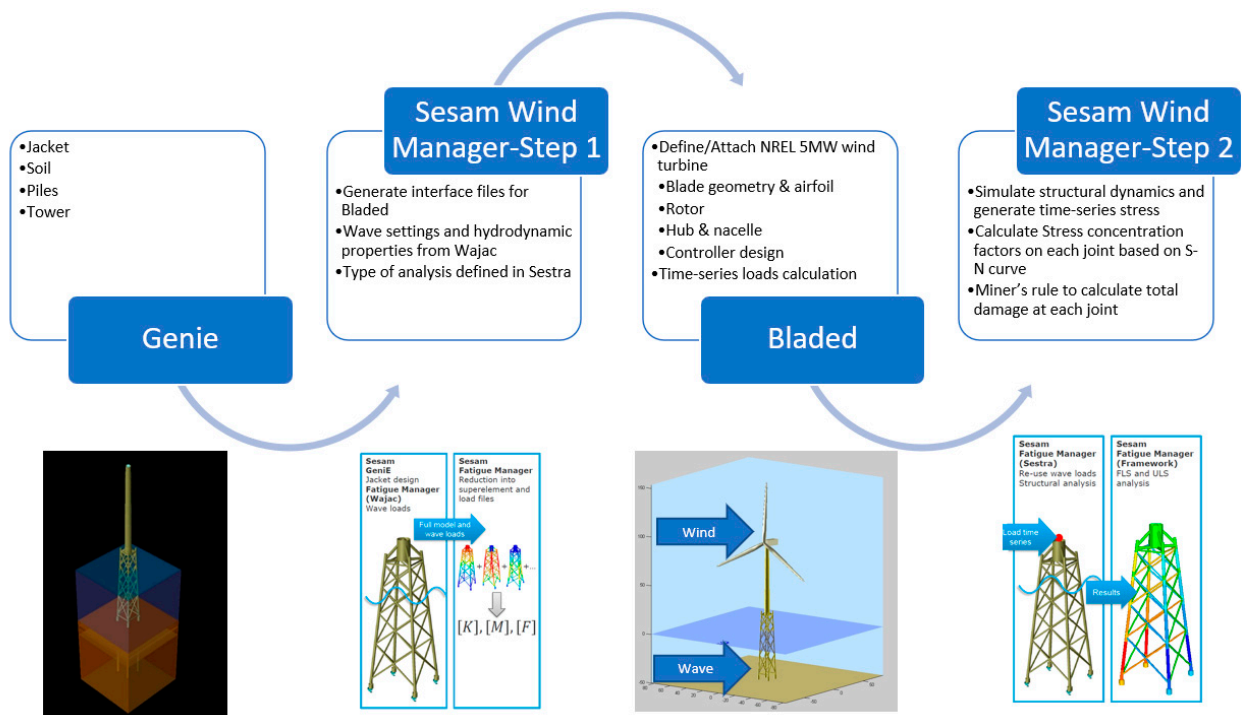**Figure 10.** Hotspots of K-joint [44].

Figure 11. Flowchart of software modules.

5. Results and Discussion

The modelling parameters significantly affect the dynamic behaviour of the jacket, which also affects the fatigue life. Optimising the stiffness-to-mass ratio by varying design parameters to reach the perfect design is a typical feature of effective structural design. It is crucial to identify the parameters affecting the dynamic behaviour of the model. The effect of modelling parameters like marine growth, flooding, soil profile, the mass TP, the material of TP, scour development, and the length of grouted connection on the dynamic response was studied and discussed below.

The effect of these design parameters was also studied on the fatigue life of the jacket foundation. For this purpose, the fatigue life was compared for all the joints. Since the jacket design has much redundancy, the fatigue life of the second worst-performing joint has been considered a failure. The location of the worst-performing joint is on the x-brace, as shown in Figure 12. The fatigue damage value of 1 represents when the jacket's crack initiates, which leads to failure. Moreover, the effect of different grouted connection configurations on the time-series fatigue life of the jacket has also been studied.

5.1. Soil

The Original OC4 jacket foundation is linear and clamped at the base without any soil. The soil profile of the site selected in the North-sea was modelled in Genie and compared with the first four natural frequencies of the original model. It can be observed that the natural frequency of all the modes is lower than that of the original model (Table 5). This phenomenon is because soil stiffness is lower, and the structural behaviour is more flexible; hence, the eigenvalue frequencies will be lower. The trend agrees with the findings of the study [46]. Figure 13 shows the dynamic response and Figure 14 shows the damage of soil and non-soil models respectively. The damage is greater when the soil non-linearity is included in the model because of the lower stiffness and higher amplitude vibrations.
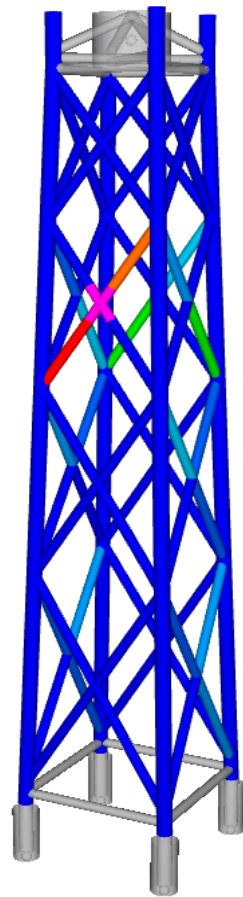
Figure 12. Location of the worst-performing joint.

	Actual	With soil
■ 1st Fore-aft	0.3169	0.2918
■ 1st Side-to-side	0.3169	0.2919
■ 2nd Fore-aft	1.1799	0.927
■ 2nd Side-to-side	1.1799	0.928

■ 1st Fore-aft ■ 1st Side-to-side ■ 2nd Fore-aft ■ 2nd Side-to-side
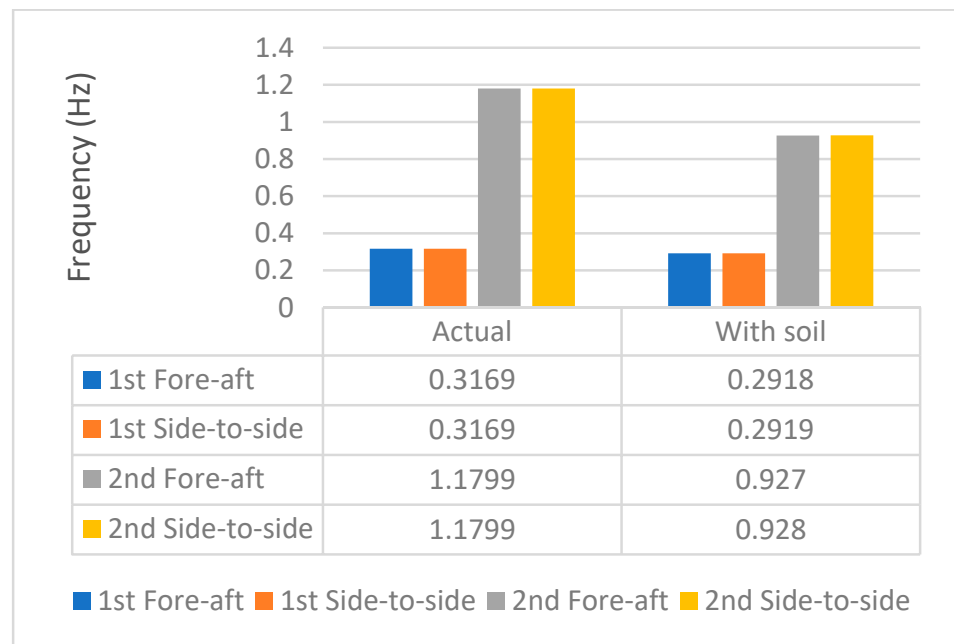
Figure 13. Dynamic response with and without soil.

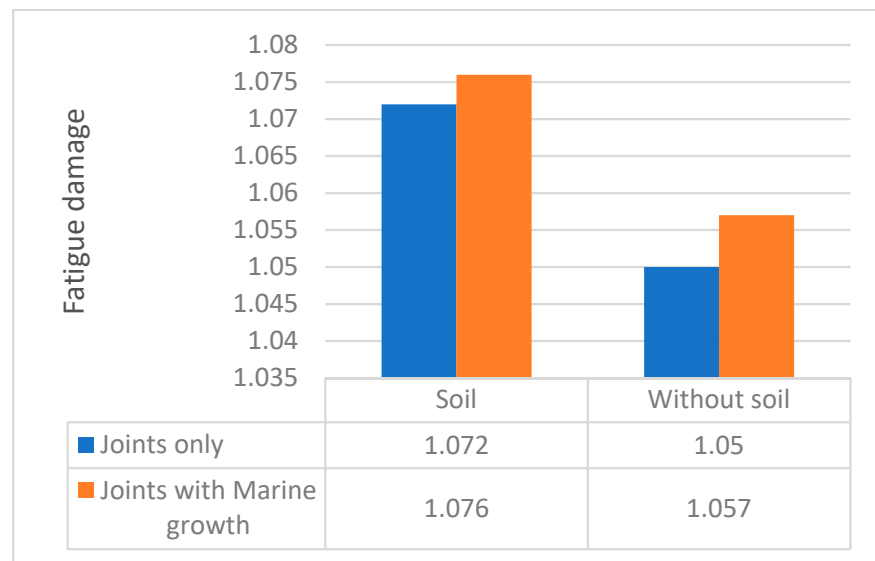|	Soil	Without soil
■ Joints only	1.072	1.05
■ Joints with Marine growth	1.076	1.057

Figure 14. Fatigue damage showing the effect of soil and marine growth.

5.2. Marine Growth

Various marine growth mechanisms develop in the submerged jacket members, affecting the structural response because of the added structural area and the change in surface roughness. The marine growth was introduced in the model from the water depth of 2 to 40 m, with an increased density of 1100 kg/m^3 and thickness of 100 mm as per the guidelines of the DNV standard. It is observed that adding the marine growth has not changed the stiffness (Figure 15), and the effect on fatigue life (Figure 14) is not significant either. The fatigue damage may be slightly greater because of the increased SCF.
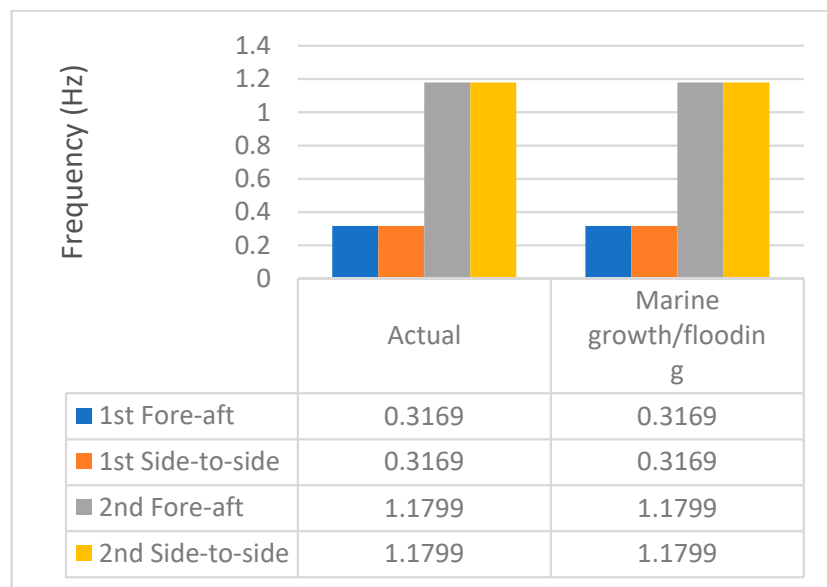

	Actual	Marine growth/flooding
■ 1st Fore-aft	0.3169	0.3169
■ 1st Side-to-side	0.3169	0.3169
■ 2nd Fore-aft	1.1799	1.1799
■ 2nd Side-to-side	1.1799	1.1799

Figure 15. Dynamic response with/without marine growth.

5.3. Transition Piece

A TP connects the jacket foundation with the tower, and its design significantly affects the dynamic response and fatigue life. Two primarily used configurations are a stiff concrete block and a light frame design. The OC4 jacket foundation has a concrete TP, but Genie can not model a concrete block. The TP was modelled as a beam with increased stiffness and an added mass of 628,107 kg to simulate a similar effect. Moreover, the impact of TP on

the dynamic response and fatigue is studied based on three configurations. The medium configuration has a mass of 314,203 kg, and No TP configuration excludes the point mass. An additional configuration was also studied by including Steel TP (actual stiffness), and its effect on fatigue life is discussed below.

The first and second natural frequencies are close to the 1P and 3P rotor frequencies and are not impacted much by the change in mass (Figure 16). This trend follows the findings given in [47]. However, the effect is significant on the third and fourth natural frequencies.
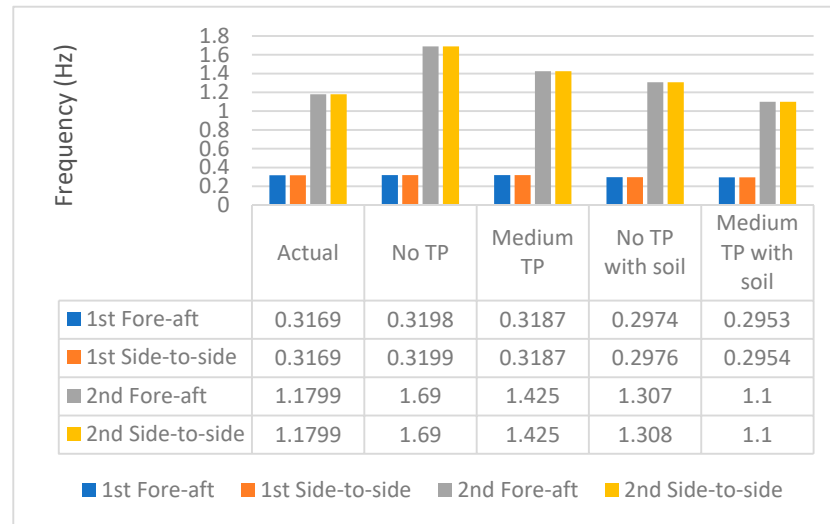
	Actual	No TP	Medium TP	No TP with soil	Medium TP with soil
■ 1st Fore-aft	0.3169	0.3198	0.3187	0.2974	0.2953
■ 1st Side-to-side	0.3169	0.3199	0.3187	0.2976	0.2954
■ 2nd Fore-aft	1.1799	1.69	1.425	1.307	1.1
■ 2nd Side-to-side	1.1799	1.69	1.425	1.308	1.1

Figure 16. Effect of transition piece on the dynamic response.

The FLS check shows that the higher mass increases the axial force and moments on the joints, hence increasing fatigue damage (Figure 17). It is also observed that the fatigue damage decreases significantly when the whole TP is made of steel. The damage is lower due to the lighter TP and the absence of irregular material change in TP, which reduces the stress on joints.
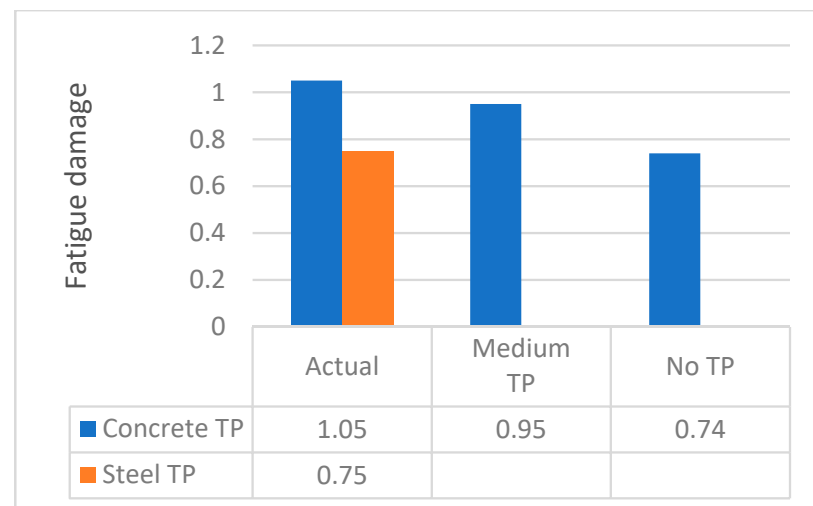
	Actual	Medium TP	No TP
■ Concrete TP	1.05	0.95	0.74
■ Steel TP	0.75		

Figure 17. Effect of transition piece on the fatigue damage.

5.4. Scour

Seabed scour occurs near the intersection of piles with the soil. Scour is governed by structural geometry, fluid flow, and seabed conditions. The study assumes that the scour has already formed and does not investigate the phenomena of scour formation because it is outside the scope of this study. Three different configurations of scour are considered, which affect the values of spring stiffness showing the soil model.

Scour can affect the structural integrity because the embedded area of the jacket is lower, which results in lower support. This phenomenon results in lower stiffness and eigenvalue frequencies. Figure 18 shows that the effect is insignificant on the first fore-aft and side-to-side frequencies. However, there is a reduction in third and fourth eigenvalue frequency. There is a reduction of 0.70, 1.32, and 3.20% for 0.5, m, and 2 m of scour, respectively.
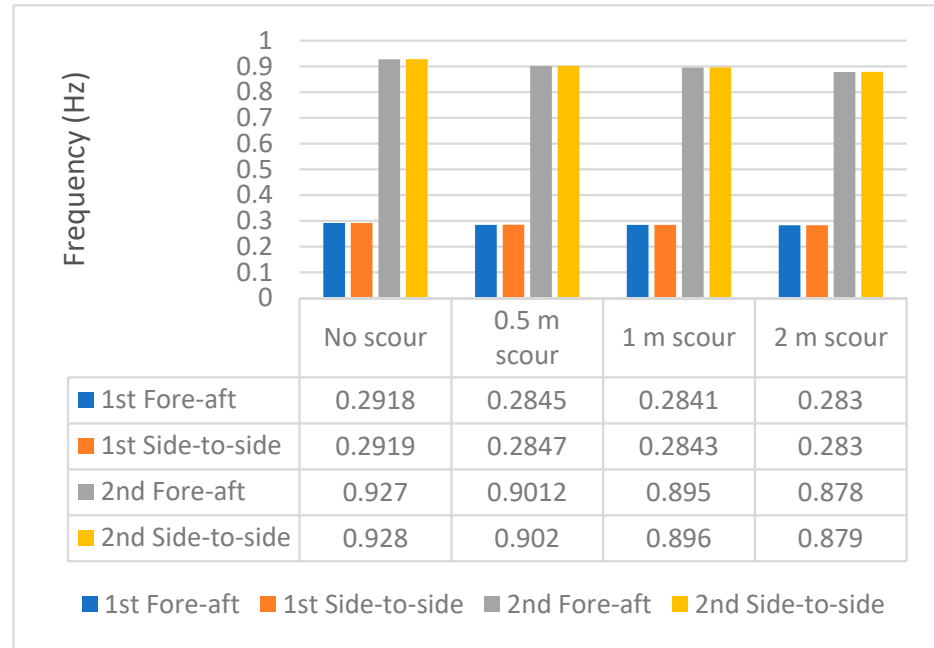
	No scour	0.5 m scour	1 m scour	2 m scour
■ 1st Fore-aft	0.2918	0.2845	0.2841	0.283
■ 1st Side-to-side	0.2919	0.2847	0.2843	0.283
■ 2nd Fore-aft	0.927	0.9012	0.895	0.878
■ 2nd Side-to-side	0.928	0.902	0.896	0.879

Figure 18. Effect of scour size on the dynamic response.

As expected, the lower support produces greater damage to the structure. The damage increases with the scour size (Figure 19) as it increases the stress range. It is worth noting that the increase in the damage with the scour size is not steep. Few soil types (low cohesion) can produce significant damage if the scour phenomenon is not mitigated. This asks for the need to perform frequent scour prevention and mitigation measures [47].
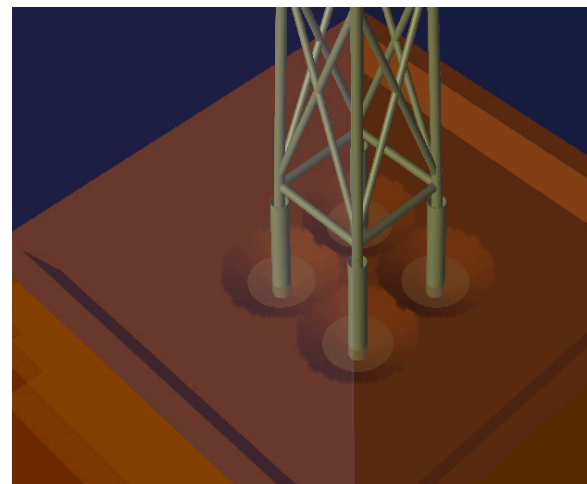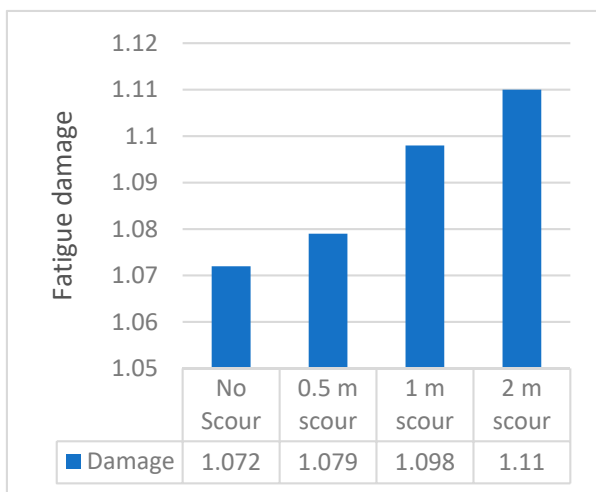
	No Scour	0.5 m scour	1 m scour	2 m scour
■ Damage	1.072	1.079	1.098	1.11

Figure 19. Effect of Scour on fatigue damage.

5.5. Grouted Connection

The OC4 jacket foundation is cantilevered at the mudline with a grouted connection. The grouted connection consists of the pile, jacket leg, and the two tubular members, and

these are connected with a grout material (density = 2000 kg/m^3) filled at each joint. The DNV practice recommends two concepts for the grouted connection design, i.e., inclined pile in leg and leg in a pile (see Figure 20). The inclined leg in the pile model has a pile diameter less than the leg, while the diameter of the pile is greater than the leg in the leg in a pile model.
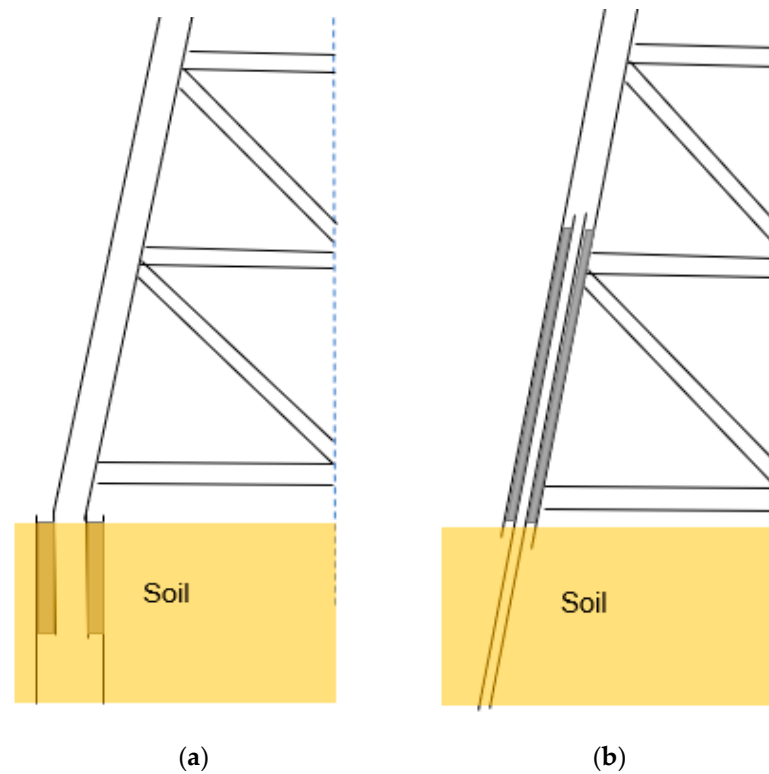

Figure 20. Types of grouted connections. (**a**) Pile in leg. (**b**) Leg in pile.

The original design of the OC4 foundation has a leg in a pile configuration, and the length of the grouted connection is 4 m. Two modified configurations of grouted connections were simulated. In one model, the length of grouted connection was increased to 6 m in the leg in a pile configuration, such that the hub height increased from 88.15 m to 90.15 m. The pile diameter was kept the same as in the original model (2.082 m). The second model has an inclined pile in leg configuration with a pile diameter of 0.9 m. The first two eigenvalue frequencies were not altered much in the leg in a pile model, but there was a decrease of 2.16% in the third and fourth natural frequencies (Figure 21). However, there was a significant decrease in the eigenvalue frequencies in the inclined pile in a leg model. The first two natural frequencies were inside the 1P rotor frequency range, which is a soft structure, as discussed in [48] and [49].

The fatigue damage has considerably reduced for the leg in a pile configuration with an increased grouted connection size (Figure 22), which is expected because it has greater support at the bottom. However, the damage is considerably greater for the inclined pile in a leg configuration because the 1P frequency is closer to the natural frequency of the rotor. Moreover, the structure is also not stiff enough to provide good support. Another interesting observation was that the highest damage point was on an x-brace around the middle of the jacket, which has moved to the braces at the bottom of the jacket. Additionally, the damage at the previous point of reference has slightly increased to 1.08.
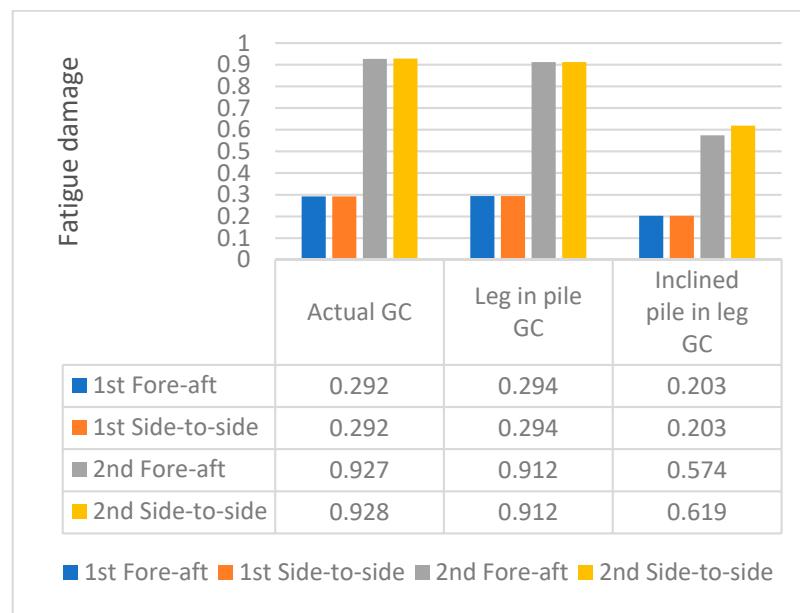
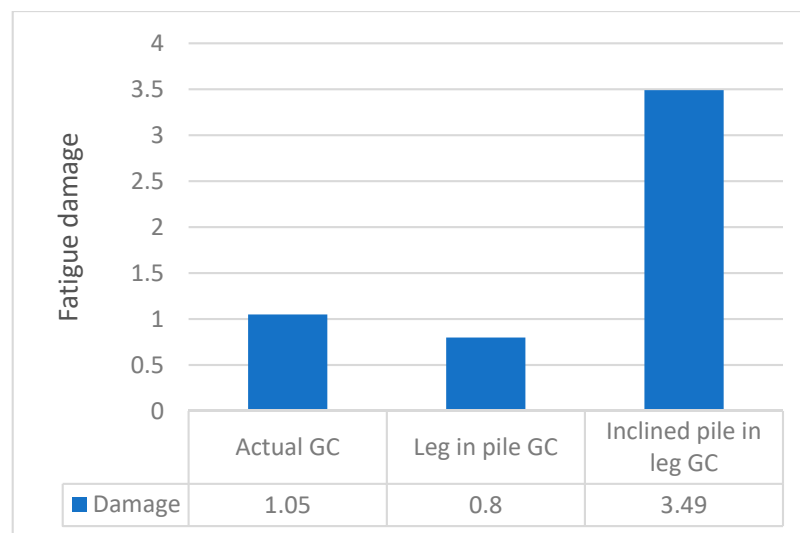**Figure 21.** Effect of grouted connection on the dynamic response.

The chart shows Fatigue damage values:

	Actual GC	Leg in pile GC	Inclined pile in leg GC
1st Fore-aft	0.292	0.294	0.203
1st Side-to-side	0.292	0.294	0.203
2nd Fore-aft	0.927	0.912	0.574
2nd Side-to-side	0.928	0.912	0.619

Figure 21. Effect of grouted connection on the dynamic response.

	Actual GC	Leg in pile GC	Inclined pile in leg GC
Damage	1.05	0.8	3.49

Figure 22. Effect of grouted connection on fatigue damage.

6. Conclusions

In this study, the effect of different parameters on the structural response of the jacket foundation was observed in terms of dynamic response and fatigue life. The OC4 jacket foundation was developed in Sesam and validated with previous research. The validated model was converted to the super-element model and exported to Bladed, where it was attached to an NREL 5-MW wind turbine. The time-series wind and wave loads were simulated in Bladed to obtain the time-series loads. These time-series loads were exported to the SWM, where FLS analyses were performed. The steps were repeated by keeping identical wind/wave loads, and the effect of marine growth, non-linearity of soil, transition piece's mass and material, scour size, and the length of grouted connection on the dynamic response and fatigue damage was observed by considering the life of 20 years. The fatigue damage of 1 implies that a crack has fully developed.

It was observed that the effect of marine growth was minimal on the structural dynamic response and fatigue damage. However, the non-linearity of the soil has a significant impact on the dynamic response. The original OC4 jacket foundation has a fixed base, and a soil profile of the north sea was included in the model. The damage of the

non-linear model is greater than the original model because of the lower stiffness of the soil model, which results in vibrations of higher amplitude. The effect of non-linearity was further extended to include the scour of different sizes (0.5, 1, and 2 m). The effect of the scour size was insignificant on the first two natural frequencies, but there was a reduction of 3.2% in the third and fourth natural frequencies for a scour of 2 m. The values reduced by 0.7% and 1.32% for the scour sizes of 0.5 and 1 m, respectively—the reduction in the support due to scour caused the damage to increase.

The study also observed the effect of changing the design in the form of the transition piece and grouted connection. The TP with three mass configurations showed that the third and fourth eigenvalue frequencies change significantly, and an inverse relationship was observed between the mass and frequencies. However, the first two frequencies were not altered. The fatigue damage was greater for the heavier TP because of the higher axial force and moments on the joints, which resulted in higher stresses. The material selection between the concrete TP and steel TP showed the need to move to the lighter steel frames to extend the fatigue life.

A unique set of simulations were performed by increasing the length of the grouted connection from the original grouted connection size of 4–6 m for a leg in a pile configuration; this resulted in the increase of the hub height to 90.15 m. The overall effect was an increase in fatigue life because of the greater support. The design configuration was also changed to an inclined pile in a leg; this resulted in the reduction of the first two eigenvalue frequencies near the 1P range. This resulted in a steep rise in fatigue damages near the lower part of the jacket. In terms of fatigue damage, marine growth has a minimum effect and can be ignored. However, the introduction of non-linearity along with scour should be included to increase the accuracy of the results. Moreover, the study recommends the need to adopt steel TP instead of concrete. The length of grouted connection for a leg in a pile configuration can be increased to increase the fatigue life.

An effort was made to minimise the simplifications in the design, which is usually the case due to the cost and complexity of such simulations. This research adds to knowledge by examining the influence of a unique combination of changes in the design, material of the transition piece, and grouted connection on dynamic response and fatigue life. The research also presents in-depth information on the sophisticated design of FLS analysis utilising the super-element approach (mostly used in industry). Future work should include the effect of turbulence intensity and wave-current to improve the results. There is also a scope to study the effect of the diameter and thickness of the members on the structural response. The parameters that can significantly impact the design life of jacket foundations were identified. This can help in extending the design life as well as reduce costs. The increased number of parameters and design changes observed in the TP and grouted connection in the complex time-series simulations significantly contribute to knowledge. The FLS analysis helps identify the weaker joints, and the damage parameter of 1 is considered a failure. However, in reality, it shows that the crack has been initiated, and the structure has not failed. Future work may include crack propagation and fracture mechanics principles to study the actual failure of the joint.

Nomenclature

OWT	Offshore Wind Turbine
NREL	National Renewable Energy Laboratory
SWM	Sesam Wind Manager
RNA	Rotor Nacelle Assembly
TP.	Transition piece
MSL	Mean Sea Level
FLS	Fatigue Limit State
DLC	Design Load Case
DOF	Degree of Freedom
SCF	Stress Concentration Factor

References

1. International Renewable Energy Agency. Future of Wind: Deployment, Investment, Technology, Grid Integration and Socio-economic Aspects a Global Energy Transformation Paper Citation about IRENA. 2019. Available online: https://www.irena.org/-/media/files/irena/agency/publication/2019/oct/irena_future_of_wind_2019.pdf (accessed on 27 April 2022).
2. Biswal, R.; Mehmanparast, A. Fatigue damage analysis of offshore wind turbine monopile weldments. *Procedia Struct. Integr.* **2019**, *17*, 643–650. [CrossRef]
3. Yeter, B.; Garbatov, Y.; Soares, C.G. Fatigue damage assessment of fixed offshore wind turbine tripod support structures. *Eng. Struct* **2015**, *101*, 518–528. [CrossRef]
4. Marjan, A.; Shafiee, M. Evaluation of Wind Resources and the Effect of Market Price Components on Wind-Farm Income: A Case Study of Ørland in Norway. *Energies* **2018**, *11*, 2955. [CrossRef]
5. Velarde, J.; Bachynski, E.E. Design and fatigue analysis of monopile foundations to support the DTU 10 MW offshore wind turbine. *Energy Procedia* **2017**, *137*, 3–13. [CrossRef]
6. Aasen, S. Soil-Structure Interaction Modelling for an Offshore Wind Turbine with Monopile Foundation. Master's Thesis, Norwegian University of Life Sciences, Akershus, Norway, 2016.
7. Aasen, S.; Page, A.; Skau, K.S.; Nygaard, T.A. Effect of the Foundation Modelling on the Fatigue Lifetime of a Monopile-based Offshore Wind Turbine. *Wind Energy Sci. Discuss.* **2016**, *2007*, 361–376. [CrossRef]
8. Byrne, B.; Mcadam, R.; Harvey, B.; Houlsby, G. PISA: New design methods for offshore wind turbine monopiles. In Proceedings of the Offshore Site Investigation Geotechnics 8th International Conference Proceeding, London, UK, 12–14 September 2017.
9. Shittu, A.; Mehmanparast, A.; Wang, L.; Salonitis, K.; Kolios, A. Comparative Study of Structural Reliability Assessment Methods for Offshore Wind Turbine Jacket Support Structures. *Appl. Sci.* **2020**, *10*, 860. [CrossRef]
10. Shittu, A.; Mehmanparast, A.; Shafiee, M.; Kolios, A.; Hart, P.; Pilario, K. Structural reliability assessment of offshore wind turbine support structures subjected to pitting corrosion-fatigue: A damage tolerance modelling approach. *Wind Energy* **2020**, *23*, 2004–2026. [CrossRef]
11. Saadian, R.; Taheri, A. Fatigue damage analysis of an existing fixed offshore platform using spectral method for life extension. *J. Mar. Sci. Technol.* **2018**, *23*, 877–887. [CrossRef]
12. Wu, Y.W. Time Domain Fatigue Life Analysis of Offshore Jacket Structure. 2019. Available online: http://asmedigitalcollection.asme.org/OMAE/proceedings-pdf/IOWTC2019/59353/V001T01A043/6464358/v001t01a043-iowtc2019-7591.pdf (accessed on 8 March 2021).
13. Shi, W.; Park, H.; Han, J.; Na, S.; Kim, C. A study on the effect of different modeling parameters on the dynamic response of a jacket-type offshore wind turbine in the Korean Southwest Sea. *Renew. Energy* **2013**, *58*, 50–59. [CrossRef]
14. Shi, W.; Park, H.C.; Chung, C.W.; Kim, Y.C. Comparison of dynamic response of monopile, tripod and jacket foundation system for a 5-MW wind turbine. In Proceedings of the International Offshore and Polar Engineering Conference, Maui, HI, USA, 19–24 June 2011; pp. 263–269. [CrossRef]
15. Kovarbašić, M.; Vorpahl, F.; Schaumann, P. Influence of structural redundancy on fatigue life of offshore wind turbine jacket structures. In Proceedings of the International Offshore and Polar Engineering Conference, Maui, HI, USA, 19–24 June 2011; pp. 274–281.
16. Tran, T.T.; Kim, E.; Lee, D. Development of a 3-legged jacket substructure for installation in the southwest offshore wind farm in South Korea. *Ocean Eng.* **2022**, *246*, 110643. [CrossRef]
17. Shi, W.; Han, J.; Kim, C.; Lee, D.; Shin, H.; Park, H. Feasibility study of offshore wind turbine substructures for southwest offshore wind farm project in Korea. *Renew. Energy* **2015**, *74*, 406–413. [CrossRef]
18. Glisic, A.; Nguyen, N.D.; Schaumann, P. Comparison of integrated and sequential design approaches for fatigue analysis of a jacket offshore wind turbine structure. In Proceedings of the International Offshore and Polar Engineering Conference, Maui, Hawaii, USA, 19–24 June 2011; pp. 440–447.
19. Glisic, A.; Nguyen, N.D.; Schaumann, P. Fatigue Analysis on Innovative 10 mw Offshore Jacket Structure Using Integrated Design Approach. In Proceedings of the International Conference on Wind Energy Harvesting, Catanzaro, Italy, 21–23 March 2018; p. 269.

20. DNV. Design of Offshore Wind Turbine Structures. 2014. Available online: https://rules.dnv.com/docs/pdf/DNV/ST/2018-07/DNVGL-ST-0119.pdf (accessed on 28 June 2021).
21. IEC. Design Requirements for Offshore Wind Turbines. 2009. Available online: https://webstore.iec.ch/preview/info_iec61400-3-1%7Bed1.0%7Den.pdf (accessed on 28 June 2021).
22. DNV. Recommended Practice Environmental Conditions and Environmental Loads. 2010. Available online: http://www.dnv.com (accessed on 28 June 2021).
23. Damiani, R.; Song, H. A jacket sizing tool for offshore wind turbines within the systems engineering initiative. *Offshore Technol. Conf. Proc.* **2013**, *3*, 2304–2330. [CrossRef]
24. Gentils, T.; Wang, L.; Kolios, A. Integrated structural optimisation of offshore wind turbine support structures based on finite element analysis and genetic algorithm. *Appl Energy* **2017**, *199*, 187–204. [CrossRef]
25. Bhattacharya, S. *Design of Foundations for OffshoreWind Turbines*; Willey: Chichester, UK, 2019.
26. Fischer, S.T.; de Vries, W. Upwind Design Basis. 2010. Available online: http://resolver.tudelft.nl/uuid:a176334d-6391-4821-8c5f-9c91b6b32a27 (accessed on 28 June 2021).
27. Jonkman, J.; Butterfield, S.; Musial, W.; Scott, G. Definition of a 5-MW Reference Wind Turbine for Offshore System Development. Golden, CO (United States). 2009. Available online: http://www.osti.gov/bridge (accessed on 10 April 2020).
28. Jonkman, J.; Musial, W. Offshore Code Comparison Collaboration (OC3) for IEA Task 23 Offshore Wind Technology and Deployment. Golden, CO (United States). 2010. Available online: https://www.osti.gov/biblio/1004009 (accessed on 10 April 2020).
29. Vorphal, F.; Kaufer, D. *Technical Report Description of a Basic model of the 'UpWind Reference Jacket' for Code Comparison in the OC4 Project under IEA Wind Annex 30*; Fraunhofer Institute for Wind Energy and Energy System Technology: Bremerhaven, Germany, 2013.
30. Abhinav, K.A.; Saha, N. Stochastic response of jacket supported offshore wind turbines for varying soil parameters. *Renew. Energy* **2017**, *101*, 550–564. [CrossRef]
31. de Mendonca, E.M.; Ellwanger, G.B.; de Sousa, J.R.M. A Comparative Study of Jacket Foundations for Offshore Wind Turbines. In Proceedings of the Ibero-Latin-American Congress on Computational Methods in Engineering, Natal, Brazil, 11-14 November 2019.
32. Damiani, R.R.; Robertson, A.N.; Jonkman, J.M. Assessing the Importance of Nonlinearities in the development of a substructure model for the wind turbine CAE tool FAST. In Proceedings of the International Conference on Offshore Mechanics and Arctic Engineering American Society of Mechanical Engineers, Nantes, France, 9–14 June 2013; Volume 55423. Available online: https://asmedigitalcollection.asme.org/OMAE/OMAE2013/volume/55423 (accessed on 28 June 2021).
33. Shi, W.; Park, H.C.; Chung, C.W.; Shin, H.K.; Kim, S.H.; Lee, S.S.; Kim, C.W. Soil-Structure Interaction on the Response of Jacket-Type Offshore Wind Turbine. *Int. J. Precis. Eng. Manuf.-Green Technol.* **2015**, *2*, 139. [CrossRef]
34. Passon, P. Damage equivalent wind-wave correlations on basis of damage contour lines for the fatigue design of offshore wind turbines. *Renew. Energy* **2015**, *81*, 723–736. [CrossRef]
35. *DNV-OS-J101*; Design of Offshore Wind Turbine Structures. DNV: Bærum, Norway, 2014.
36. *IEC 61400-3*; Design Requirements for Offshore Wind Turbines. IEC: Geneva, Switzerland, 2009.
37. DNV GL. *Fixed Offshore Wind What Sesam Can Do for Fixed Offshore Wind Turbine*; DNV GL: Bærum, Norway, 2018.
38. Glisic, A.; Nguyen, N.D.; Schaumann, P. Fatigue Analysis on Innovative 10 mw Offshore Jacket. In Proceedings of the WINER-COST'18 International Conference on Wind Energy Harvesting, Catanzaro, Italy, 21–23 March 2018; pp. 297–300.
39. DNV. *Using Sesam TM and Bladed in One Workflow*; DNV: Bærum, Norway, 2021.
40. DNV. *Verification Report of Sesam's Bladed Interface_Implementing an Interface between Bladed and Sesam Verification*; DNV: Bærum, Norway, 2019.
41. Manolas, I.; Riziotis, V.A.; Papadakis, G.P.; Voutsinas, S.G. Hydro-Servo-Aero-Elastic Analysis of Floating Offshore Wind Turbines. *Fluids* **2020**, *5*, 200. [CrossRef]
42. DNV. *BLADED, Engineering Feature Summary*; DNV: Bærum, Norway, 2020.
43. *IEC 61400-1*; Wind Turbines—Design Requirements. IEC: Geneva, Switzerland, 2005.
44. DNV GL. *Fatigue Design of Offshore Steel Structures RP-C203*; DNV GL: Bærum, Norway, 2014.
45. Glisic, A.; Ferraz, G.T.; Schaumann, P. Sensitivity Analysis of Monopiles' Fatigue Stresses to Site Conditions Using Monte Carlo Simulation. In Proceedings of the 27th (2017) International Ocean and Polar Engineering Conference, ISOPE 17, San Francisco, CA, USA, 25–30 June 2017.
46. Hung, Y.C.; Chang, Y.Y.; Chen, S.Y. Natural frequency and vibration analysis of jacket type foundation for offshore wind power. *IOP Conf. Ser. Mater. Sci. Eng.* **2017**, *276*, 012035. [CrossRef]
47. Martinez-Luengo, M.; Kolios, A.; Wang, L. Parametric FEA modelling of offshore wind turbine support structures: Towards scaling-up and CAPEX reduction. *Int. J. Mar. Energy* **2017**, *19*, 16–31. [CrossRef]
48. Arany, L.; Bhattacharya, S.; Macdonald, J.H.G.; Hogan, S.J. Closed form solution of Eigen frequency of monopile supported offshore wind turbines in deeper waters incorporating stiffness of substructure and SSI. *Soil Dyn. Earthq. Eng.* **2016**, *83*, 18–32. [CrossRef]
49. Miceli, F. Wind Farms Construction. 2017. Available online: https://www.windfarmbop.com/type-of-towers-stiff-soft-or-soft-soft/ (accessed on 15 July 2022).